



Experimental Study of Neodymium (Nd^{3+}) Doped Mn-Ni based Spinel Ferrite ($\text{Mn}_{0.5}\text{Ni}_{0.5}\text{Nd}_x\text{Fe}_{2-x}\text{O}_4$) Nanoparticle using Sol-Gel Method

Zaheer Abbas Gilani¹, Muhammad Waqas Tariq¹, H. M. Noor ul Huda Khan Asghar^{1*}, Naeem Khan¹

¹ Department of Physics, Balochistan University of Information Technology, Engineering & Management Sciences, Quetta 87300, Pakistan

ARTICLE INFO

Article History:

Received: October 07, 2021
Revised: December 11, 2021
Accepted: December 30, 2021
Available Online: December 31, 2021

Keywords:

Spinel Ferrite
Neodymium
Nanocrystallite Ferrites
XRD
Sol-gel
Dielectric Properties

ABSTRACT

Neodymium (Nd^{3+}) doped Mn-Ni based spinel ferrite with composition of $\text{Mn}_{0.5}\text{Ni}_{0.5}\text{Nd}_x\text{Fe}_{2-x}\text{O}_4$ ($x = 0.00, 0.5, 0.10, 0.15$ and 0.20), the nanoparticle was essentially formulated by sol-gel self-ignition method. The impact of Nd^{3+} doping on structural and electrical properties has been extensively studied. XRD verified the FCC spinel arrangement of the synthesized samples. The Debye Scherer formula is used to determine the crystalline size, which was observed in the nano scale ranging between 6 and 10 nm. XRD was used to validate the composition, crystalline size and determining different structural parameters of sample. It is noted that the lattice parameter changes when the Nd^{3+} doping concentration was enhanced because smaller radius of Fe^{3+} ions is replaced by large ionic radius of Nd ions. When Nd concentration raises X-Ray density and dislocation density also rises. FTIR verify the compositions of spinel phase and also examine the absorption bands. There were two major frequency bands one was high frequency band ν_1 with range of about 500cm^{-1} . Second was low frequency band ν_2 with range of about almost 400cm^{-1} . Dielectric performed in the frequency range of 1 MHz to 3 GHz. It was used to determine the effect of Nd^{3+} doping on various parameters. Dielectric investigations showed decline in dielectric constant. Impedance analysis revealed reducing values with frequency, due to the increase in material conductivity. Real and imaginary modulus study showed the influence of grain boundaries at low frequencies. These properties played significant role in high frequency applications and semiconductor devices.



© 2021 The Authors, Published by iRASD. This is an Open Access article under the Creative Common Attribution Non-Commercial 4.0

*Corresponding Author: noorulhudakhan@gmail.com

1. Introduction

Magnetic material which has both electrical and magnetic nature is known ferrite. The ferrite materials with iron oxide and metal oxide shows different and unique properties which are used in electrical, magnetic, electronic and electrochemical fields (Chavan, Babrekar, More, & Jadhav, 2010; Goldman, 2006). Spinel ferrites are a class of oxide materials having an incredibly rare mix of electric and magnetic characteristics. Spinel ferrite exhibit superb features like, high frequency, strangely high electrical resistance and high saturation magnetization (Adam, Davis, Dionne, Schloemann, & Stitzer, 2002). Nanocrystalline spinel ferrite (NCSF) show massive attraction due to their amazing physical and chemical properties related to bulk material. Spinel ferrite nanoparticle are greatly important to scientists and researches due to their extraordinary applications, electronic produces microwave, television, home appliances, media recording radio and communication. More applications are in different field like medical diagnoses, magnetic

refrigeration, water purification and Ferro-fluids (Maaz, Mumtaz, Hasanain, & Ceylan, 2007; Song & Zhang, 2004). To enhance magnetic and electrical properties of spinel ferrite the rare earth material has been doped because they have stable valency and large radius (Roy & Bera, 2006). Basically Mn and Ni are soft magnetic material which have a lot of applications in different fields of life such as in electronic devices, transformer core, and high frequency applications (Azadmanjiri, 2008; Mathe & Kamble, 2008). Neodymium (Nd^{3+}) is doped with Mn-Ni based spinel ferrite which causes structural spoil and development of electrical magnetic properties and also rise density, electrical resistance, high eddy current and reduce the saturation magnetization and electrical loss because Neodymium has unpaired electrons in outermost shell (4f orbit) which increase to iron with non-magnetic nature. Neodymium ions have big ionic radii which replaces iron (Fe) ion at octahedral site of ferrite, resulting in high-frequency application while improving the magnetic and electrical property of spinel ferrite (B. Chauhan, Kumar, Jadhav, & Singh, 2004; Wang, Chen, Zeng, & Hou, 2004). These characteristics of spinel ferrite depend on nature, type of dopants and also depend on synthesis method and placement of cations over the vacant interstitial sites (Gilani, Warsi, Khan, et al., 2015). The objective of this article is to examine the effects of Neodymium ion doping on structural, electric, dielectric properties and magnetic characteristics of Mn-Ni based spinel ferrites, as well as their suitability for transferring high frequency applications and memory storage devices.

2. Experimental Procedure

Mn-Ni based spinel ferrite nanoparticles were prepared by sol-gel method using Manganese (II), Nickel (II) and neodymium (Nd^{3+}). The manganese nickel ferrite doping with rare earth element (Nd^{3+}) with different concentration ($x = 0.00, 0.5, 0.10, 0.15, 0.20$). The chemical material with analytical form was utilized as crude agent to prepare necessary ferrite nanomaterial. The substance contained nickel nitrate [$\text{Ni}(\text{NO}_3)_2 \cdot 6\text{H}_2\text{O}$], manganese nitrate [$\text{Mn}(\text{NO}_3)_2 \cdot 4\text{H}_2\text{O}$], Ferric nitrate [$\text{Fe}(\text{NO}_3)_3 \cdot 9\text{H}_2\text{O}$] and citric acid [$\text{C}_6\text{H}_8\text{O}_7 \cdot \text{H}_2\text{O}$] which were mixed in distilled water to achieve a homogeneous solution. The solution was placed on the hot plates at temperature 80°C with magnet stirrer at 400 rpm to dry until the sol was formed. After a while, sol transformed into a black high dense gel. The solution was regularly stirred and the hotplate the temperature began to raise steadily enhanced up 150°C . The gel burnt in response to the self-spreading exothermic oxidation reaction. The final product was obtained in the form of homogenous fluffy dry powder. The fine powder was then annealed for four hours at 600 degree Celsius to produce the materials' hexagonal phase. After that the prepared samples were analyzed by using XRD analysis crystalline structures. It gives information about structures morphology, grain size, shape, strain and desired crystalline perspectives. The angle range of 2θ is from 10° to 80° . FTIR verify the compositions of spinel phase in each formulation and provides information about chemical variations and cation distribution. FTIR spectra range was observed between ($400\text{-}1000\text{ cm}^{-1}$). Dielectric was used to determine the effect of Nd^{3+} doping on various parameters such as the A.C conductivity, real and imaginary parts of the modulus, impedance, dielectric constant, electric modulus, and Loss tangent was analyzed at frequencies ranging from 1 MHz to 3 GHz.

3. Results and Discussion

3.1. XRD Analysis

The Sol-gel method was used to prepare XRD arrangement of $\text{Mn}_{0.5}\text{Ni}_{0.5}\text{Nd}_x\text{Fe}_{2-x}\text{O}_4$ ($x = 0.0, 0.05, 0.10, 0.15, 0.20$) spinel ferrites. The phase of crystallization of the specimens was annealed at 600°C for 4 hours. XRD was used to validate the composition and crystal size. The crystalline phase of the prepared specimen was verified by XRD measurements. XRD has really promising approach for determining different structural parameters of materials of various compositions, such as Crystallite size, lattice strain, lattice constant, x-Ray density, unit cell volume, bulk density, micro-strain, stacking fault and dislocation density (A. Chauhan & Chauhan, 2014). The XRD graph of all spinel ferrite samples are shown in fig 1. The data shows that at $2\theta = 35^\circ$, extremely intense peaks value with 311 hkl form, which is a great peak for spinel ferrites nano-particles. The peaks that are kept in contact with the XRD trend are recorded as (220), (311), (400), (331), (422), (333), (440) and (531). All of These peaks relate to FCC spinel structure peaks, indicating that the ferrite was made up of FCC spinel structure, as verified by JCPDS card. According to the XRD study, all of the specimens have distinct sharp peaks. All of the reported peaks were wide,

indicating that the ferrite was nanocrystalline. A pair of secondary peaks can be seen, one of which is at $2\theta = 44.5$ and has an hkl value of 411, and the other is at $2\theta = 32.9$. These secondary peaks could be caused by Nd insolubility in the octahedral location (Gilani, Warsi, Anjum, et al., 2015).

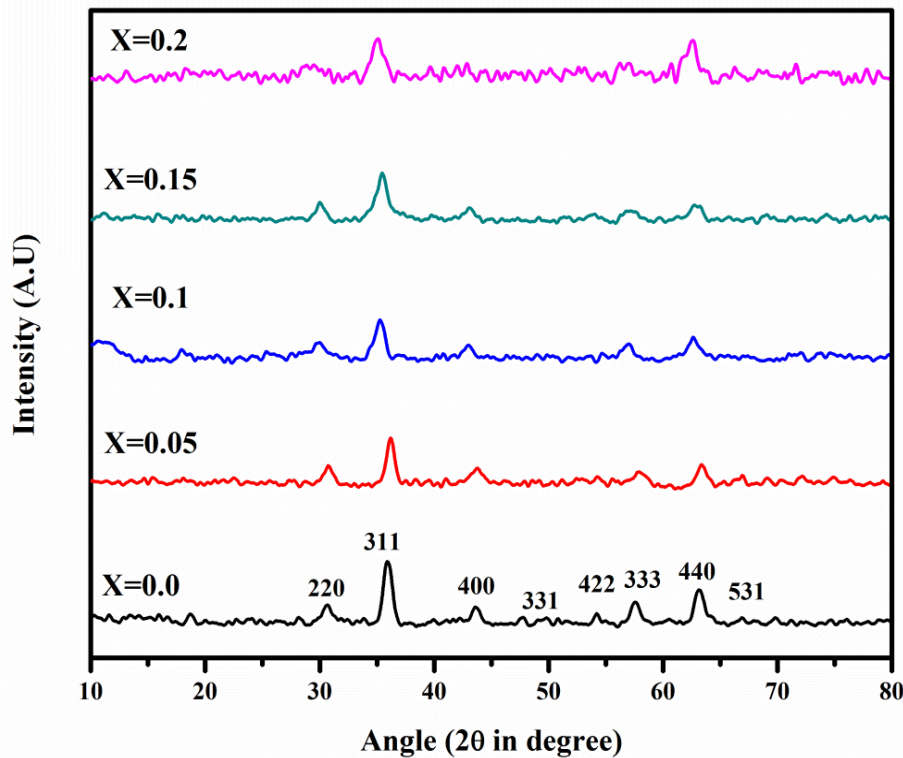


Figure 1: XRD pattern of $Mn_{0.5}Ni_{0.5}Nd_xFe_{2-x}O_4$ ($x = 0.0, 0.05, 0.10, 0.15, 0.20$)

Table 1
Different structural parameters of $Mn_{0.5}Ni_{0.5}Nd_xFe_{2-x}O_4$ ($x = 0.0, 0.05, 0.10, 0.15, 0.20$)

Parameter	X=0.0	X=0.05	X=0.10	X=0.15	X=0.20
Crystalline size(nm)	8.518	10.763	6.501	8.341	6.228
Lattice constant	8.2862	8.2816	8.3300	8.3452	8.3246
Cell volume	568.9495	568.0029	578.0189	581.1807	576.8996
Bulk density	1.42203	1.54089	1.61890	1.431309	1.342516
X-ray density	5.41696	5.51954	5.53881	5.60011	5.75680

3.1.1. Crystalline Size vs Concentration

The average crystalline size of the formulated ferrite substance was calculated using XRD. The crystalline size was used to determine the hkl value of (311) by Debye sherrer's equation

$$D_m = k\lambda / \beta \cos\theta \tag{1}$$

There k is the constant whose value is 0.9. λ representing the wavelength which is equal to 1.54\AA , β represents the worth of the angle of an extreme peak with FWHM, and θ represents the angle of scattering of the most extreme peak. The crystalline size was calculated to become very small ranging between 6 and 10 nanometers. It was observed that the crystalline size differed in-homogeneously with the doping of Nd^{3+} . This crystalline size in-homogeneity possible that this is due to the creation of a impurity phase., as well as the comparatively small ionic radius of Nd^{3+} relative to the Fe^{2+} to be substituted (Vijayabhaskar, Rajmohan, Vignesh, & Venkatakrisnan, 2019). The crystalline size difference can be seen on the graph below.

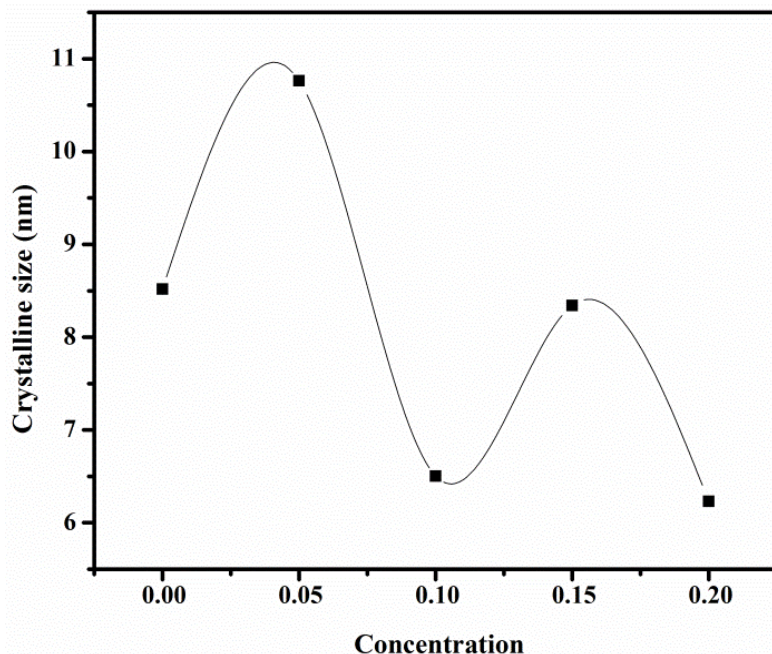


Figure 2: Crystalline size vs Nd Concentration $Mn_{0.5}Ni_{0.5}Nd_xFe_{2-x}O_4$ ($x = 0.0, 0.05, 0.10, 0.15, 0.20$)

3.1.2. Lattice Constant vs Concentration

Nelson Relay method was used to determine the lattice parameter.

$$a = d (h^2 + K^2 + l^2)^{1/2} \tag{2}$$

The average lattice constant was found between the range of 8.28 to 8.32 Å. The foundation of Nd^{3+} and Fe^{3+} ion radius changes as the value of the "a" changes. It's important to note that the lattice parameter decreases when the Nd^{3+} ion substrate is doped. It's because the Fe^{3+} ion's massive radius has been replaced (0.76 Å) at the octahedral positions by small orbit of an Nd ion. The lattice constant declines rapidly with doping at first, then increases, then decreases again. This may be expected for Nd^{3+} ion separation at grain boundaries. The following graph depicts the difference in the lattice parameter.

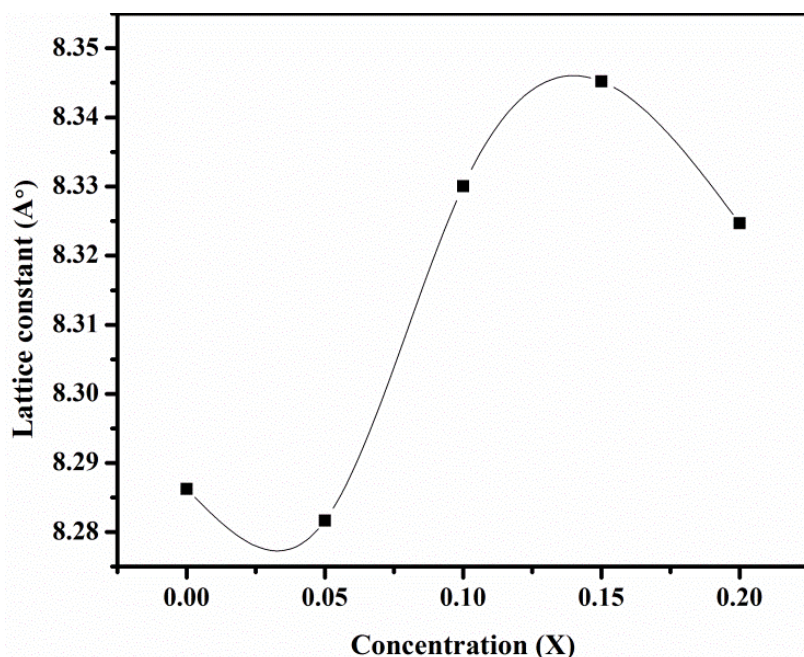


Figure 3: Lattice constant vs concentration $Mn_{0.5}Ni_{0.5}Nd_xFe_{2-x}O_4$ ($x = 0.0, 0.05, 0.10, 0.15, 0.20$)

3.1.3.X-Ray Density vs Concentration

The equation below can be used to measure the x-ray density of formulated spinel ferrite.

$$D_x = 8M/Na^3 \tag{3}$$

Here M indicates the sample's molecular weight, 8 denote the number of formulation units, N represents "Avogadro's number" of 6.0223×10^{23} , and "a" represents lattice constant. The difference of X-Ray density with comparison to concentration ranges from 5.41 to 5.75 gm/cm³. The relationship between X-Ray density and concentration is considered to be mostly static. When Nd concentration raises X-Ray density also raises, which is due to higher molar weight of Nd³⁺ (144.242) relative to Fe (55.845). A graph depicting the increases in X-ray density as a behavior of Nd concentration is seen below.

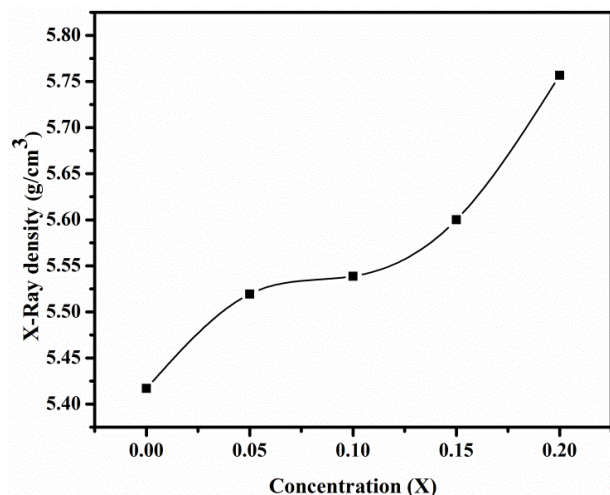


Figure 4: X-ray density vs concentration Mn_{0.5}Ni_{0.5}Nd_xFe_{2-x}O₄ (x = 0.0, 0.05, 0.10, 0.15, 0.20)

3.1.4.Bulk Density vs Concentration

Bulk density of specimen was used to analyze the following equation,

$$\rho_m = m/v \tag{4}$$

Here "m" is mass and volume is denoted by "v". Bulk density varies between 1.34 and 1.61 gm/cm³. It is estimated to be much lower than X-Ray density. The in-homogeneous variance of bulk density is noted; it raises first, then declines steadily with concentration (Ortega-Zúñiga et al., 2019).

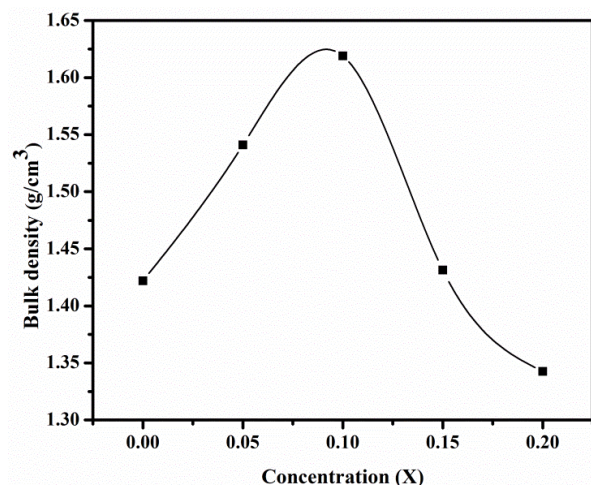


Figure 5: Bulk density vs concentration Mn_{0.5}Ni_{0.5}Nd_xFe_{2-x}O₄ (x = 0.00, 0.05, 0.10, 0.15 and 0.20)

3.1.5. Lattice Strain vs Concentration

The Stokes-Wilson formula was used to measure the lattice strain of the synthesized nano-particles.

$$\epsilon = \beta/4 \tan \theta (10^{-3}) \tag{5}$$

β shows the FWHM of intense peak. The lattice strain was estimated between 13.19×10^3 and 18.06×10^3 . The lattice strain dropped at first, then enhanced, decrease and finally began to enhanced w.r.t the doping concentration. At the value of $x = 0.20$, the maximal value of lattice strain was observed (Wu et al., 2019). The graph below depicts variations in lattice strain as a function of concentration:

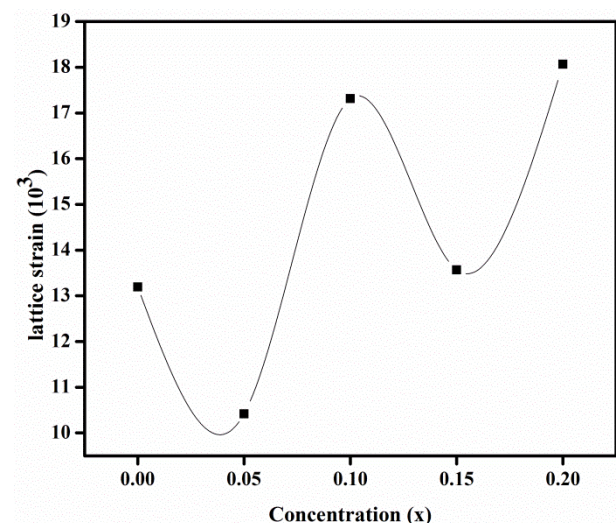


Figure 6: Lattice Strain vs Concentration $Mn_{0.5}Ni_{0.5}Nd_xFe_{2-x}O_4$ ($x = 0.0, 0.05, 0.10, 0.15, 0.20$)

3.1.6. Micro Strain vs Concentration

The given equation calculates the micro-strain of the synthesized samples.

$$\text{Micro-strain} = (\beta \cos \theta)/4 (10^{-3}) \tag{6}$$

The micro strain was calculated between the ranges 4.06×10^{-3} and 5.56×10^{-3} . It was estimated to be rising in a discontinuous nature in relation to the doping concentration. The maximum possible value of micro-strain is identified at $x = 0.20$. The following graph depicts shifts in micro-strain w.r.t concentration.

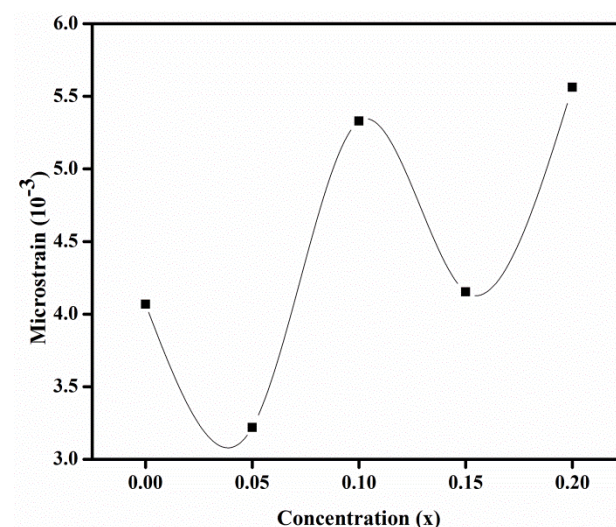


Figure 7: Micro-strain vs. Concentration $Mn_{0.5}Ni_{0.5}Nd_xFe_{2-x}O_4$ ($x = 0.0, 0.05, 0.10, 0.15, 0.20$)

3.1.7. Dislocation Density vs Concentration

The dislocations density of formulated spinel ferrites is obtained by the following equation

$$\delta = 1/D^2 (10^{15}) \quad (7)$$

Where D represents the crystalline size of sample. The dislocations density is obtained in the range from 13.78×10^{15} to 25.77×10^{15} . It was noticed that dislocation density raised when the doping concentration of Nd was enhanced. At $x = 0.20$ the maximum value of dislocation density was determined. Graph of dislocation density is given below:

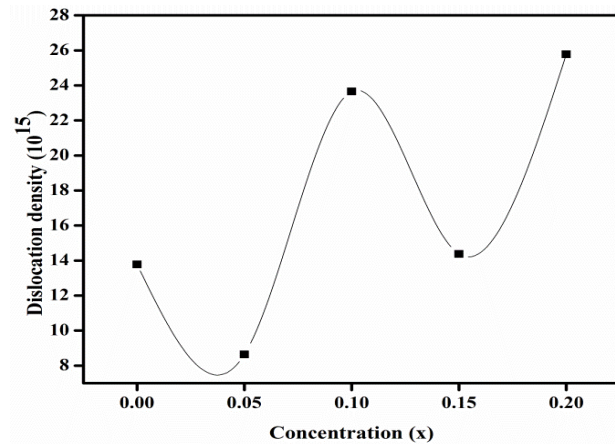


Figure 8: Dislocation Density vs. Concentration $Mn_{0.5}Ni_{0.5}Nd_xFe_{2-x}O_4$ ($x = 0.0, 0.05, 0.10, 0.15, 0.20$)

3.1.8. Stacking Fault vs Concentration

Stacking fault equation is given below:

$$\text{Stacking fault (SF)} = 2\pi^2/45\sqrt{3} (\tan \theta) \quad (8)$$

Initially a decrease was noticed in the stacking fault, it gradually increased up to some values ($x=0.15$) and then decreases once more. It's possible that the inhomogeneous behavior was caused by the temperature increase. This behavioral arrangement is depicted in the figure 9.

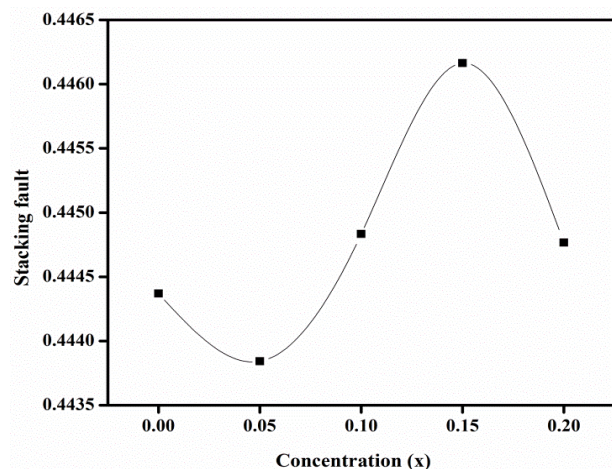


Figure 9: Stacking Fault vs Concentration $Mn_{0.5}Ni_{0.5}Nd_xFe_{2-x}O_4$ ($x = 0.0, 0.05, 0.10, 0.15, 0.20$)

Table 2

Shows the different values of lattice strain, bulk density micro-strain and stacking fault

Parameter	X=0.00	X=0.05	X=0.10	X=0.15	X=0.20
Lattice strain	13.191457	10.4179588	17.316864	13.569587	18.069548
Microstrain	4.0676247	3.21932616	5.329642	4.1537960	5.5627974
Dislocation density	13.780826	8.63223949	23.658634	14.370896	25.773892
Stacking fault	0.444369	0.44384172	0.444833	0.446163	0.444766

3.2. FTIR

FTIR verifies the compositions of spinel phase in each formulation and provides information about chemical variations and cation distribution. The FTIR verifying the spinel structure composition of sample was $Mn_{0.5}Ni_{0.5}Nd_xFe_{2-x}O_4$. There were two major frequency bands one was high frequency band ν_1 with range of about 500cm^{-1} and second was low frequency band ν_2 with range of almost 400cm^{-1} . we investigated the tetrahedral and octahedral frequency bands. The absorption peaks also known as High frequency bands were caused by the tetrahedral site of internal metal spreading vibrations, whereas low frequency bands were caused by octahedral-metal stretching bands (Mori, Imazeki, Tsutsui, & Tanahashi, 2019). Fig.10 exhibit FTIR spectra range observed between ($400\text{-}1000\text{ cm}^{-1}$)

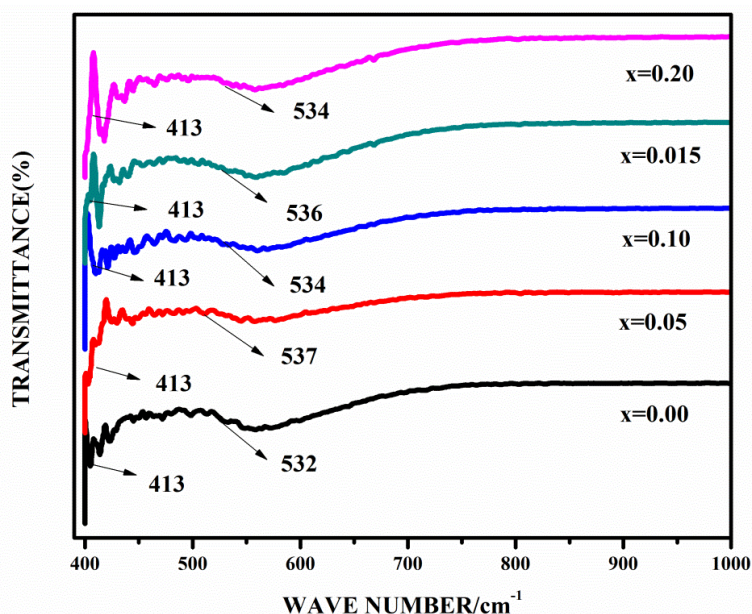


Figure 10: FTIR Frequency bands of of $Mn_{0.5}Ni_{0.5}Nd_xFe_{2-x}O_4$

The fig. shows the bands of the spinel structure's characteristic. The variation in higher frequency band was found in the range of $532\text{-}537\text{ cm}^{-1}$. However, lower frequency band were found to remain unchanged with range of about 413 cm^{-1} . The stretching vibration of $Fe^{3+}\text{-}O^{2-}$ at tetrahedral and octahedral sites formed the higher frequency and lower frequency bands. The location of the band varies with the doping of Nd^{3+} . The change in the lattice parameter causes the ν_1 frequency band shift a little bit to the high frequency. These variations affected the stretching vibration of $Fe^{3+}\text{-}O^{2-}$ and as a result, of band location can change.

Table 3

Frequency bands of FTIR $Mn_{0.5}Ni_{0.5}Nd_xFe_{2-x}O_4$ ($x = 0.00, 0.5, 0.10, 0.15$ and 0.20)

S.No	Composition	ν_1/cm^{-1}	ν_2/cm^{-1}
1	$Mn_{0.05}Ni_{0.5}Fe_2O_4$	534	413
2	$Mn_{0.05}Ni_{0.5}Nd_{0.05}Fe_{1.95}O_4$	536	413
3	$Mn_{0.05}Ni_{0.5}Nd_{0.10}Fe_{1.90}O_4$	534	413
4	$Mn_{0.05}Ni_{0.5}Nd_{0.15}Fe_{1.85}O_4$	537	413
5	$Mn_{0.05}Ni_{0.5}Nd_{0.20}Fe_{1.80}O_4$	532	413

3.3. Dielectric Measurements

The dielectric properties of arranged spinel ferrite samples with formulation of $Mn_{0.5}Ni_{0.5}Nd_xFe_{2-x}O_4$ ($x = 0.0, 0.5, 0.10, 0.15, 0.20$) was investigated using an impedance analyzer. Dielectric properties of fabricated spinel ferrites are identified at frequencies ranging from 1 MHz to 3 GHz. These properties play a significant role and are essential due to their uses in high frequency products. These characteristics are extremely dependent on the ways used for the preparation of the material's configuration and cations position (Bibi et al., 2018). Various dielectric parameters are mentioned in table 4.

3.3.1. Dielectric Constant and Permit Loss

The dielectric constant and permit loss change as a frequency behavior from 1 MHz to 3 GHz. The dielectric constant reduces as the frequency rises, as seen in Fig. 5. $Mn_{0.5}Ni_{0.5}Nd_xFe_{2-x}O_4$ ($x = 0.00, 0.05, 0.10, 0.15$ and 0.20) almost all spinel ferrite samples showed a steady reduction in the dielectric constant, and all ferrites showed vibration peaks at higher frequencies. The dielectric constant and permit loss showed distribution when the frequency was enhanced.

According to Maxwell Wagner interfacial polarization the grains are much more impressive at high frequencies, whereas at lower frequency the grain boundaries values are more impressive. The process of sintering cause's polarization between the two surfaces at low frequencies and dipolar are at high frequencies due to the spontaneous scattering of atoms of oxygen at grain boundary and grains (Mustaqeem et al., 2020). The polarization was dampened as the frequency was increased. With increasing frequency, the dielectric constant reduces. Electrons are the primary charge carriers in ferrites, and electron motion occurs b/w $Fe^{2+} - Fe^{3+}$ atoms located at octahedral sites. This is called hopping method. The transfer of electrons b/w $Fe^2 - Fe^3$ anions at the octahedral site causes a reduction in dielectric constant which rises as frequency rises, and this interchange cannot obey the alteration in an alternating current electric charge. In spinel ferrites, only a few more vibration peaks were found when electron transfer b/w $Fe^2 - Fe^3$ atoms was similar to the given AC frequency. The jumping chance of the both ions was the same if atom has double static conditions C and D that are distinguished by a wall. The frequency which interchanges the position of particle is known as the particle's real frequency. If the internal and external frequencies are equal, then the most electrical energy received the vibrating atom and the loss of influence enhanced. As a consequence, the process of resonance occurred (Junaid et al., 2016). As seen in fig.11.

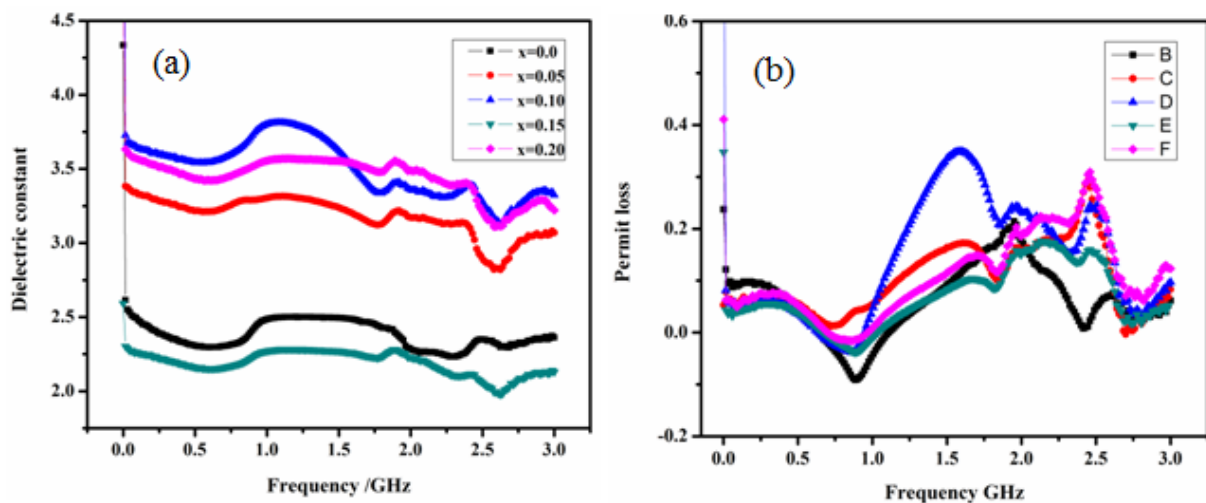


Figure 11: (a) Shows Dielectric constant vs frequency and (b) shows the permit loss vs frequency $Mn_{0.5}Ni_{0.5}Nd_xFe_{2-x}O_4$ ($x = 0.0, 0.05, 0.10, 0.15, 0.20$)

3.3.2. Tangent Loss and AC Conductivity

The ratio derived from the relationship between current loss and charging is called Tangent loss. The change in Tangent loss with frequency for $Mn_{0.5}Ni_{0.5}Nd_xFe_{2-x}O_4$ ($x = 0.0, 0.05, 0.10, 0.15, 0.20$) shown in fig.12. The frequency has inverse relation to the tangent loss. It's clear that when the frequency was increased, the amount of tangent loss decreased (Cheng et al., 2018). At lower frequency, electrons' hopping frequency matched the applied field, and loss was relatively high. As the applied field frequency was raised then frequency of hopping b/w $Fe^{2+}-Fe^{3+}$ atom couldn't obey the external field over a particular critical frequency, resulting in a significant reduction in loss. As the doping of rare-earth element Nd^{3+} increased Peaks drifted into the lower frequency zone. The resonance frequency was reduced when the doping amount was elevated above a certain amount.

The quantity of electric current in a specimen of material is known as AC conductivity. The relationship between AC conductivity and frequency of spinel ferrites is illustrated in fig.13. AC conductivity graph shows that all samples had the same pattern at low frequencies. The high frequency area exhibited dispersion activity. According to Koop's principle and the Maxwell model the ferrites substance are made up of executing grains distinguished by grain boundaries. However, at higher frequencies, the grains are disturbed, and the hopping process b/w $Fe^{2+}-Fe^{3+}$ atom is enhanced, resulting in increased conductivity (Farid, Ahmad, Ali, Mahmood, & Ramay, 2018).

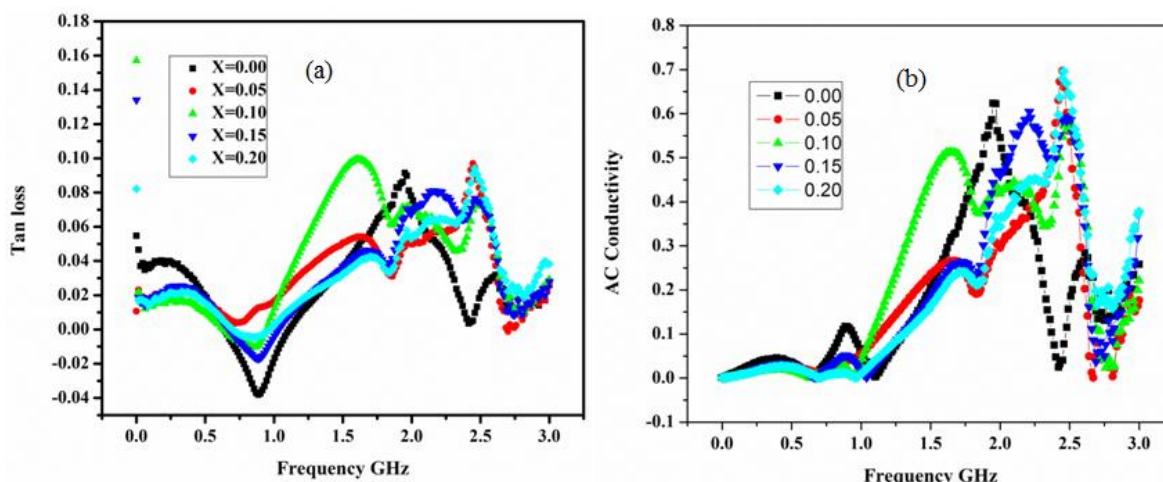


Figure 12: (a) shows Tangent loss vs Frequency and (b) shows AC conductivity vs Frequency of $Mn_{0.5}Ni_{0.5}Nd_xFe_{2-x}O_4$ ($x = 0.0, 0.05, 0.10, 0.15, 0.20$)

Table 4

Dielectric different parameters for $Mn_{0.5}Ni_{0.5}Nd_xFe_{2-x}O_4$

Parameter	Frequency	X= 0.00	X= 0.05	X= 0.10	X= 0.15	X= 0.20
Dielectric Constant	1 MHz	4.3349	4.9557	6.0769	2.59196	4.9987
	1 GHz	2.4859	3.3059	3.8020	2.27187	3.5560
	3 GHz	2.3623	3.06931	3.3240	2.12862	3.2209
Dielectric loss	1 MHz	0.2371	0.05282	0.9550	0.34757	0.4107
	1 GHz	-0.0413	0.05562	0.0482	-0.00852	0.0105
	3 GHz	0.0612	0.08288	0.0972	0.05972	0.1233
Tan Loss	1 MHz	0.0547	0.01065	0.1571	0.13409	0.0821
	1 GHz	-0.016	0.01682	0.0126	-0.00375	0.0029
	3 GHz	0.0259	0.02700	0.0292	0.02805	0.0382
AC Conductivity	1 MHz	0.0006852	0.0002578	0.0004026	0.0005562	0.0006001
	1 GHz	0.0565968	0.0566898	0.0443532	0.0139568	0.0114884
	3 GHz	0.2581030	0.1764998	0.2214708	0.3735365	0.3775462

3.3.3. Real (Z') and Imaginary (Z'') Part of Impedance

The impedance analysis can be used to fully comprehend the electrical nature of spinel ferrites. We use various representations to describe the complex plane, such as electric modulus, permittivity impedance, admittance and dielectric loss etc. Impedance performance as the frequency range was 1MHz' to 3GHz. The impedance of the formulated

spinel ferrites raised with increasing rare-earth ions Nd^{3+} doping. Z' and Z'' rise with the doping of rare-earth element, but as the frequency of the external field rises, Z' and Z'' components of impedance follow the same pattern as impedance, as seen in fig.14. The use of rare-earth ions obstructs electron transfer between the tetrahedral and octahedral sites. The impedance of the processed spinel ferrites reduced as the frequency of the applied field enhanced from 1MHz to 3GHz, as seen in fig.14. The conductivity operating system is exposed to hopping.

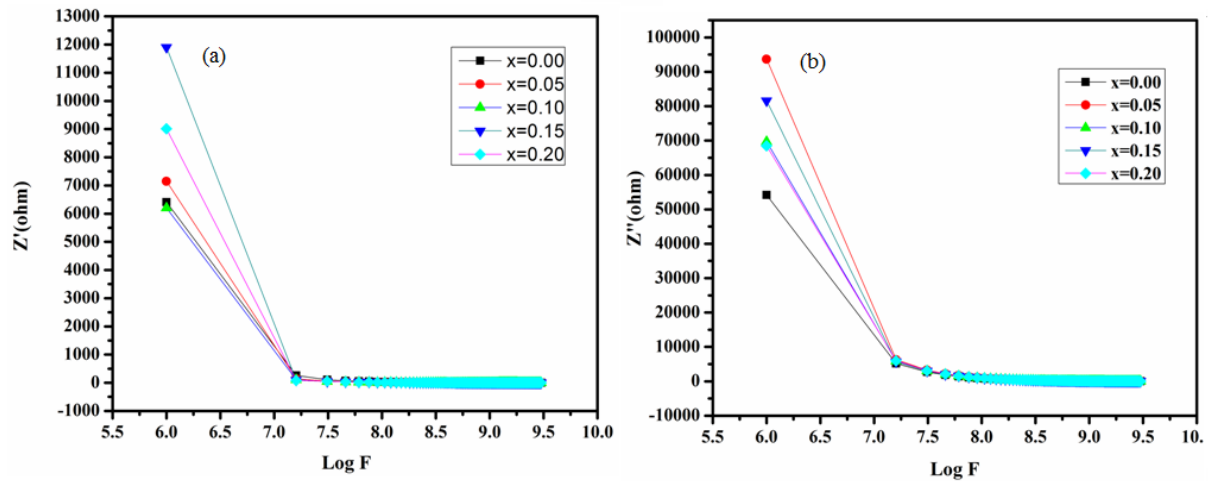


Figure 14: (a) Shows the Real (Z') part of Impedance vs. frequency and fig. (b) Shows the Imaginary (Z'') part of Impedance vs. frequency

3.3.4. Real and Imaginary Parts of Modulus

The real (M') and imaginary (M'') module of spinel ferrite formed according to configuration $Mn_{0.5}Ni_{0.5}Nd_xFe_{2-x}O_4$ were computed as the product of the applied frequency. Impedance analysis was used to investigate the position of grains and also its boundaries in the range of frequencies of 1MHz to 3GHz. Electrical reaction dependent on electric polarization phenomenon on the basis of complex electric modulus parsimony, the bulk grain and grain boundary effects in certain homogeneous materials can be defined. If the grain boundaries area takes up a lot of space, the graph between M' and M'' will reveal a lot about the semicircle. This type of approach is verified by a relationship between grain boundaries and peak formation (Khera & Chand, 2019). The existence of a peak can be seen in the graph of imaginary electric modulus vs frequency. The M' and M'' factor vs the frequency of the applied field was obtained accordingly. The M' and M'' factor have really low values at low frequencies and rise uniformly as the frequency implemented fields rise, whereas they reach highest values at higher frequencies (3GHz) can be seen in fig.15.

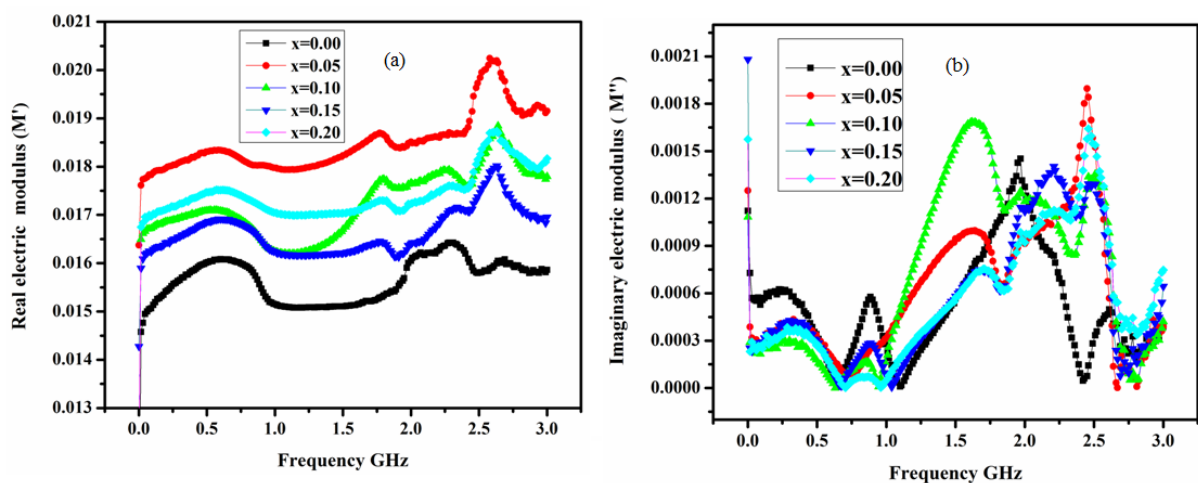


Figure 15: (a) Real (M') parts of modulus vs of frequency and fig. (b) Was Imaginary (M'') parts of modulus vs frequency of $Mn_{0.5}Ni_{0.5}Nd_xFe_{2-x}O_4$

Table 5
The different parameters values of dielectric $Mn_{0.5}Ni_{0.5}Nd_xFe_{2-x}O_4$

Parameters	frequency	X= 0.0	x = 0.05	x = 0.10	x = 0.15	x = 0.20
Z'/ohm	1 MHZ	6.41E+03	7.15E+03	6.20E+03	1.19E+04	9.01E+03
	1 GHZ	1.32E+00	1.86E+00	1.19E+00	3.74E-01	3.39E-01
	3 GHZ	7.42E-01	7.40E-01	8.02E-01	1.23E+00	1.43E+00
Z''/ohm	1 MHZ	5.42E+04	9.37E+04	6.97E+04	8.16E+04	6.85E+04
	GHZ	8.61E+01	1.02E+02	9.24E+01	9.23E+01	9.69E+01
	3 GHZ	3.02E+01	3.65E+01	3.39E+01	3.23E+01	3.46E+01
M'	1 MHZ	0.0094757	0.0163736	0.0121886	0.0142733	0.0119817
	1 GHZ	0.0151428	0.0179712	0.0162394	0.0162265	0.0170421
	3 GHZ	0.0158596	0.0191519	0.0177978	0.0169551	0.0181704
M''	1 MHZ	0.0011212	0.0012497	0.0010836	0.00208	0.00157513
	1 GHZ	0.000232	0.0003273	0.0002091	6.568E-05	5.9633E-05
	3 GHZ	0.0003892	0.000388	0.0004205	0.0006443	0.00074805

4. Conclusions

Neodymium (Nd^{3+}) doped $Mn_{0.5}Ni_{0.5}Nd_xFe_{2-x}O_4$ spinel ferrite nanoparticles were successfully prepared by sol-gel self-ignition method which has been established to be the one of simplest and quickest method for the synthesis of ferrites. Various characterizations have been used to examine the effect of Nd^{3+} doping such as XRD, FTIR and dielectric. XRD verified the crystalline phase and FCC spinel arrangement of the synthesized samples. The crystalline size was determined by sherrer's formula. It was observed in the nano scale ranging between 6 and 10 nanometers. It was observed that the crystalline size differed inhomogeneously with the doping of Nd^{3+} . XRD determining different structural parameters of sample, such as lattice strain, lattice constant, x-Ray density, unit cell volume, bulk density, micro-strain, stacking fault and dislocation density. The lattice parameter changed when the Nd^{3+} doping concentration was enhanced because smaller radius of Fe^{3+} ions is replaced by large ionic radius of Nd ions. FTIR verified the cations distribution and investigated the tetrahedral and octahedral frequency bands. Dielectric properties of fabricated spinel ferrites were identified at frequencies ranging from 1 MHz to 3 GHz. Dielectric was used to determine the effect of Nd^{3+} doping on various parameters such as the A.C conductivity, real and imaginary parts of the modulus, impedance, dielectric constant, electric modulus, and tangent loss was analyzed. These properties play a significant role and essential due to their uses in high frequency products. Dielectric investigations showed decline in dielectric constant. Impedance analysis exhibited a reducing value with frequency, due to the increase in material conductivity. Real and imaginary modulus study showed the influence of grain boundaries at low frequencies. These dielectric properties suggested that these materials could be used in high-frequency applications and semiconductor devices.

Acknowledgement

We are grateful to ORIC of Balochistan University of Information Technology, Engineering and Management Sciences (BUIITEMS), Quetta Pakistan.

References

- Adam, J. D., Davis, L. E., Dionne, G. F., Schloemann, E. F., & Stitzer, S. N. (2002). Ferrite devices and materials. *IEEE Transactions on Microwave Theory and Techniques*, 50(3), 721-737.
- Azadmanjiri, J. (2008). Structural and electromagnetic properties of Ni-Zn ferrites prepared by sol-gel combustion method. *Materials Chemistry and Physics*, 109(1), 109-112.
- Bibi, K., Ali, I., Farid, M. T., Mahmood, A., Ramay, S. M., & Ali, K. (2018). Electric and dielectric properties of ytterbium substituted spinel ferrites. *Journal of Materials Science: Materials in Electronics*, 29(5), 3744-3750.
- Chauhan, A., & Chauhan, P. (2014). Powder XRD technique and its applications in science and technology. *J Anal Bioanal Tech*, 5(5), 1-5.
- Chauhan, B., Kumar, R., Jadhav, K., & Singh, M. (2004). Magnetic study of substituted Mg-Mn ferrites synthesized by citrate precursor method. *Journal of magnetism and magnetic materials*, 283(1), 71-81.

- Chavan, S., Babrekar, M., More, S., & Jadhav, K. (2010). Structural and optical properties of nanocrystalline Ni–Zn ferrite thin films. *Journal of Alloys and Compounds*, 507(1), 21-25.
- Cheng, Y., Li, Z., Li, Y., Dai, S., Ji, G., Zhao, H., . . . Du, Y. (2018). Rationally regulating complex dielectric parameters of mesoporous carbon hollow spheres to carry out efficient microwave absorption. *Carbon*, 127, 643-652.
- Farid, H. M. T., Ahmad, I., Ali, I., Mahmood, A., & Ramay, S. M. (2018). Structural and dielectric properties of copper-based spinel ferrites. *The European Physical Journal Plus*, 133(2), 1-12.
- Gilani, Z. A., Warsi, M. F., Anjum, M. N., Shakir, I., Naseem, S., Riaz, S., & Khan, M. A. (2015). Structural and electromagnetic behavior evaluation of Nd-doped lithium-cobalt nanocrystals for recording media applications. *Journal of Alloys and Compounds*, 639, 268-273.
- Gilani, Z. A., Warsi, M. F., Khan, M. A., Shakir, I., Shahid, M., & Anjum, M. N. (2015). Impacts of neodymium on structural, spectral and dielectric properties of LiNi_{0.5}Fe₂O₄ nanocrystalline ferrites fabricated via micro-emulsion technique. *Physica E: Low-dimensional Systems and Nanostructures*, 73, 169-174.
- Goldman, A. (2006). *Modern ferrite technology*: Springer Science & Business Media.
- Junaid, M., Khan, M. A., Iqbal, F., Murtaza, G., Akhtar, M. N., Ahmad, M., . . . Warsi, M. F. (2016). Structural, spectral, dielectric and magnetic properties of Tb–Dy doped Li-Ni nano-ferrites synthesized via micro-emulsion route. *Journal of Magnetism and Magnetic Materials*, 419, 338-344.
- Khera, S., & Chand, P. (2019). Influence of different solvents on the structural, optical, impedance and dielectric properties of ZnO nanoflakes. *Chinese journal of physics*, 57, 28-46.
- Maaz, K., Mumtaz, A., Hasanain, S., & Ceylan, A. (2007). Synthesis and magnetic properties of cobalt ferrite (CoFe₂O₄) nanoparticles prepared by wet chemical route. *Journal of magnetism and magnetic materials*, 308(2), 289-295.
- Mathe, V., & Kamble, R. (2008). Anomalies in electrical and dielectric properties of nanocrystalline Ni–Co spinel ferrite. *Materials Research Bulletin*, 43(8-9), 2160-2165.
- Mori, T., Imazeki, H., Tsutsui, G., & Tanahashi, M. (2019). Evaluation of nano particle slurries by osmotic pressure measurement and its application to fabrication process of nano composite materials. *Nano-Structures & Nano-Objects*, 18, 100306.
- Mustaqeem, M., Mahmood, K., Saleh, T. A., ur Rehman, A., Ahmad, M., Gilani, Z. A., & Asif, M. (2020). Synthesis of CuFe_{2-x}Er_xO₄ nanoparticles and their magnetic, structural and dielectric properties. *Physica B: Condensed Matter*, 588, 412176.
- Ortega-Zúñiga, C., Pinzón-De la Rosa, C., Román-Ospino, A. D., Serrano-Vargas, A., Romañach, R. J., & Méndez, R. (2019). Development of near infrared spectroscopic calibration models for in-line determination of low drug concentration, bulk density, and relative specific void volume within a feed frame. *Journal of pharmaceutical and biomedical analysis*, 164, 211-222.
- Roy, P., & Bera, J. (2006). Effect of Mg substitution on electromagnetic properties of (Ni_{0.25}Cu_{0.20}Zn_{0.55})Fe₂O₄ ferrite prepared by auto combustion method. *Journal of magnetism and magnetic materials*, 298(1), 38-42.
- Song, Q., & Zhang, Z. J. (2004). Shape control and associated magnetic properties of spinel cobalt ferrite nanocrystals. *Journal of the American Chemical Society*, 126(19), 6164-6168.
- Vijayabhaskar, S., Rajmohan, T., Vignesh, T., & Venkatakrishnan, H. (2019). Effect of nano SiC particles on properties and characterization of Magnesium matrix nano composites. *Materials Today: Proceedings*, 16, 853-858.
- Wang, J., Chen, Q., Zeng, C., & Hou, B. (2004). Magnetic-field-induced growth of single-crystalline Fe₃O₄ nanowires. *Advanced Materials*, 16(2), 137-140.
- Wu, Y., Chen, Z., Nan, P., Xiong, F., Lin, S., Zhang, X., . . . Pei, Y. (2019). Lattice strain advances thermoelectrics. *Joule*, 3(5), 1276-1288.